The Travelling Wave Multipole Field Electro-Magnetic Launcher: a SOVP Analytical Model

A. Musolino*, R. Rizzo* and E. Tripodi*

* Department of Energy and System Engineering, University of Pisa, Italy, via Diotisalvi, 2, 56100, Pisa,
Email: {musolino; rocco.rizzo; ernesto.tripodi}@dsea.unipi.it

***Abstract*—The problem of the evaluation of eddy currents induced in a conductive cylinder is here reconsidered under the light of possible application in the electromagnetic launch context. In particular we derive an analytical solution when the system is excited by a sinusoidal current flowing in a saddle coil moving in the axial direction. Subsequently we consider an arrangement of such coils distributed in the axial and azimuth direction. When properly fed they produce a travelling wave of flux distribution which is able to exert a thrust force on the conductive cylinder. Since the governing vector field equation is not separable in the cylindrical coordinates, an approach based on the second order vector potential (SOVP) formulation has been here adopted. Scalar field equations are obtained whose solutions are expressed in terms of Bessels functions.**

I. Introduction

In recent papers [1], [2] a revisited version of the reconnection launcher [3] has been presented under the name of Multipole Field Electromagnetic Launcher. This launcher is an induction device and as a consequence is free from the drawbacks related to the sliding contacts that affect the rail launchers. With respect to the conventional Linear Induction Launcher (LIL), it is characterized by a better ratio of the radial compression force to the axial thrust force. Currents in the armature of LIL are induced by the variation of the axial component of the flux density, but this component of the flux density produces an intense radial force [4]. The axial thrust force is associated with the radial components of the flux density which is smaller than the axial component. In the multipole configuration each driving coils produces a magnetic field that is mainly directed along the radius of the cylinder. The resultant effect of the action of the coils distributed in the azimuth direction is the production of a loop current around the cylinder. Interaction of the radial magnetic flux density with this loop eddy current produces a large axial thrust force, while the radial compressive force becomes smaller [1]. Other interesting features are contactless magnetic suspension, potential super-velocity launch and large mass driven. This last feature makes this launcher a candidate for vehicle propulsion and for space transportation development. The analysis performed in [1], [2] is purely numerical and refers to a three-stages device operating in pulse mode. In this paper we propose an analytical model of the device operating in a travelling wave mode. The armature is a conductive hollow cylinder indefinitely extended in the direction of the motion, while the stator coils are substantially arranged as shown in [1]. In the proposed analysis the number of coils in the motion direction, as well as in the azimuth direction can be arbitrary. The analytical model is based on the evaluation of the electromagnetic quantities (fields everywhere and induced current in the conductive cylinder) produced by a single stator coil (saddle shaped) when it carries a sinusoidal current and moves at constant velocity in the axial direction with respect to the cylinder. When dealing with 3D problems and especially in curvilinear coordinated the separation of variables is not always possible. In these cases the use of the second-order vector potentials appropriately approaches the problem [6]-[9]. The problem is reformulated by using scalar equations and the solutions are written in terms of ordinary and modified Bessels functions of the first and second kind. The availability of an analytical solution has a twofold utility: 1) allows a deep understanding of the operation of the device and of its potentialities and drawbacks; 2) constitutes a benchmark for the validation of numerical codes that are indispensable in the analysis of real devices [5], [10].

However, the proposed formulation can be used also for the investigation of magnetic levitation systems [11].

The paper is organized as follows: in Section II the problem setup is discussed in detail. Section III reports the formulation and the solution of the governing equation in terms of SOVP and Section IV reports an example of an application.

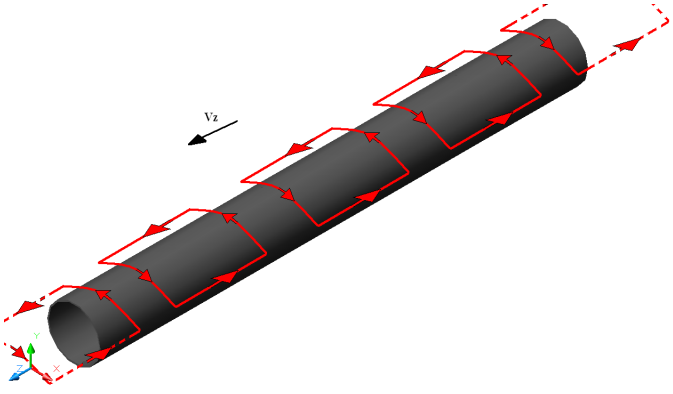

Fig. 1. The analyzed system.

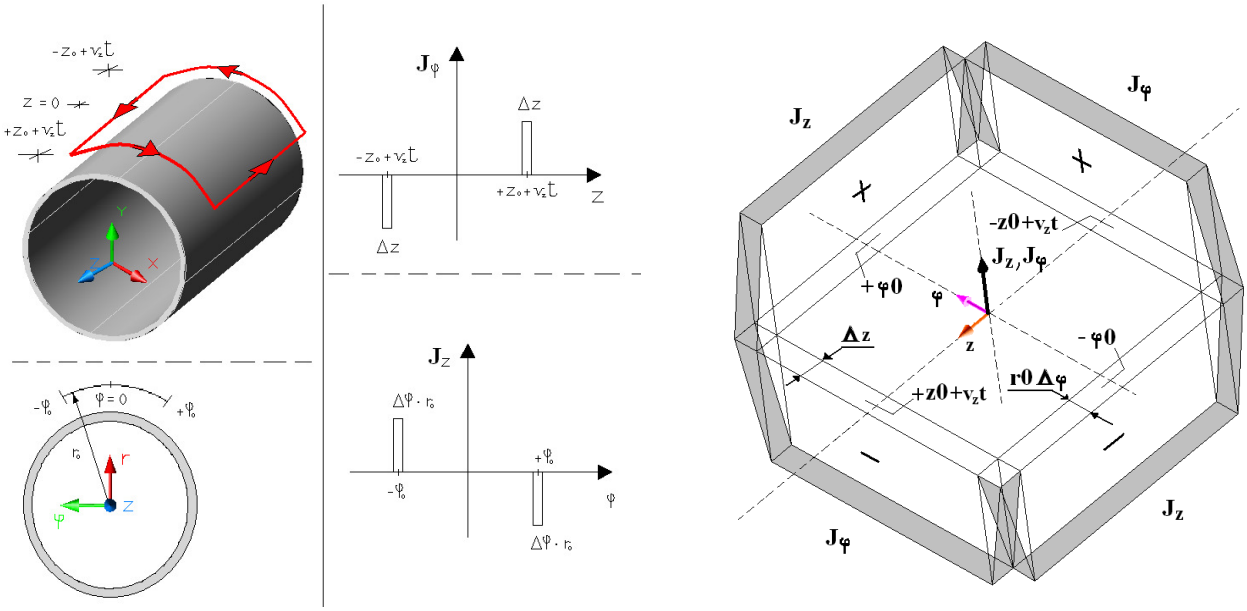

(a) coil arrangement

(b) current profile (schematic)

Fig. 2. Schematic view of the system with a single exciting coil.

$$\tilde{J}_\varphi(\varphi,z) = J\cdot\left\{\frac{1}{\Delta_\varphi}\left(\varphi-\left(-\varphi_0-\frac{\Delta_\varphi}{2}+c_\varphi\right)\right)\cdot u\left(\varphi-\left(-\varphi_0-\frac{\Delta_\varphi}{2}+c_\varphi\right)\right)-\frac{1}{\Delta_\varphi}\left(\varphi-\left(-\varphi_0+\frac{\Delta_\varphi}{2}+c_\varphi\right)\right)\cdot u\left(\varphi-\left(-\varphi_0+\frac{\Delta_\varphi}{2}+c_\varphi\right)\right)+\right.$$
$$\left.-\frac{1}{\Delta_\varphi}\left(\varphi-\left(\varphi_0-\frac{\Delta_\varphi}{2}+c_\varphi\right)\right)\cdot u\left(\varphi-\left(\varphi_0-\frac{\Delta_\varphi}{2}+c_\varphi\right)\right)+\frac{1}{\Delta_\varphi}\left(\varphi-\left(\varphi_0+\frac{\Delta_\varphi}{2}+c_\varphi\right)\right)\cdot u\left(\varphi-\left(\varphi_0+\frac{\Delta_\varphi}{2}+c_\varphi\right)\right)\right\}\times$$
$$\times\left\{\left[u\left(z-\left(-z_0-\frac{\Delta_z}{2}+k_z\right)\right)-u\left(z-\left(-z_0+\frac{\Delta_z}{2}+k_z\right)\right)\right]-\left[u\left(z-\left(z_0-\frac{\Delta_z}{2}+k_z\right)\right)-u\left(z-\left(z_0+\frac{\Delta_z}{2}+k_z\right)\right)\right]\right\};$$

$$\tilde{J}_z(\varphi,z) = J\cdot\left\{\frac{1}{\Delta_z}\left(z-\left(-z_0-\frac{\Delta_z}{2}+k_z\right)\right)\cdot u\left(z-\left(-z_0-\frac{\Delta_z}{2}+k_z\right)\right)-\frac{1}{\Delta_z}\left(z-\left(-z_0+\frac{\Delta_z}{2}+k_z\right)\right)\cdot u\left(z-\left(-z_0+\frac{\Delta_z}{2}+k_z\right)\right)+\right.$$
$$\left.-\frac{1}{\Delta_z}\left(z-\left(z_0-\frac{\Delta_z}{2}+k_z\right)\right)\cdot u\left(z-\left(z_0-\frac{\Delta_z}{2}+k_z\right)\right)+\frac{1}{\Delta_z}\left(z-\left(z_0+\frac{\Delta_z}{2}+k_z\right)\right)\cdot u\left(z-\left(z_0+\frac{\Delta_z}{2}+k_z\right)\right)\right\}\times$$
$$\times\left\{\left[u\left(\varphi-\left(\varphi_0+\frac{\Delta_\varphi}{2}+c_\varphi\right)\right)-u\left(\varphi-\left(\varphi_0-\frac{\Delta_\varphi}{2}+c_\varphi\right)\right)\right]-\left[u\left(\varphi-\left(-\varphi_0+\frac{\Delta_\varphi}{2}+c_\varphi\right)\right)-u\left(\varphi-\left(-\varphi_0-\frac{\Delta_\varphi}{2}+c_\varphi\right)\right)\right]\right\};$$

where J is the current density magnitude, and the terms c_φ and $k_z = c_z + v_z t$ are used to properly locate the current sheet along the φ and z directions and to take into account its movement along the z-direction.

II. Description of the Problem

The analyzed system is schematically shown in Fig. 1. A conductive cylinder is located inside a fictitious coaxial cylindrical surface; an array of moving coils (in the axial direction) is attached on this surface. A number of these arrays of coils can be located at different angular positions. As a result a matrix of coils lying on this fictitious surface surrounds the conductive cylinder. Coils at the same axial position are fed with the same sinusoidal current. The phase shift of the currents in coils at different axial positions varies linearly with the z-coordinate and a traveling wave of flux density is produced. As a result a thrust force is exerted on the conductive cylinder in the direction of the travelling wave. As known this force is a function of the relative speed between cylinder and the coils and of the travelling wave speed. The solution of the proposed problem can be written by superposition of the solution obtained for the elementary arrangement shown in Fig. 2, where only one coil fed with a sinusoidal current is present and the cylinder moves at constant speed in the axial direction. The radial dimension of the coil is assumed to be negligible and the coil is approximated by a ribbon whose geometry and position is shown in figs. 2(a) and 2(b). However, if this hypothesis falls, the coils system can be approximated by stacking in the radial direction a proper number of ribbons. Then, due to the linearity of the system, the solution of the problem can be evaluated by using the superposition principle.

In cylindrical coordinates the current sheet is written as:

$$\mathbf{J}(\varphi,z,t) = \tilde{J}_\varphi(\varphi,z)\,e^{j\omega t}\cdot\mathbf{a}_\varphi + \tilde{J}_z(\varphi,z)\,e^{j\omega t}\cdot\mathbf{a}_z \quad (1)$$

where $\tilde{J}_\varphi$ and $\tilde{J}_z$ are shown in Fig. 2.

A double Fourier transform in the axial and in the azimuth directions is then performed:

$$\begin{aligned}\tilde{J}_\varphi(\varphi,z) &= \sum_{m=-\infty}^{+\infty}\sum_{n=-\infty}^{+\infty} K'^{\varphi}_{mn} e^{j\alpha_m\varphi} e^{j\beta_n z} \\ \tilde{J}_z(\varphi,z) &= \sum_{m=-\infty}^{+\infty}\sum_{n=-\infty}^{+\infty} K'^{z}_{mn} e^{j\alpha_m\varphi} e^{j\beta_n z}\end{aligned} \tag{2}$$

where: $\alpha_m = 2\pi m/T_\varphi$; $\beta_n = 2\pi n/T_z$, T_z and T_φ respectively represent the axial and azimuth period of the current distribution, and:

$$K'^{\varphi}_{mn} = \frac{1}{T_\varphi T_z}\int_{-\frac{T_\varphi}{2}}^{\frac{T_\varphi}{2}}\int_{-\frac{T_z}{2}}^{\frac{T_z}{2}} \tilde{J}_\varphi(\varphi,z)\, e^{-j\alpha_m\varphi} e^{-j\beta_n z} d\varphi dz$$

$$K'^{z}_{mn} = \frac{1}{T_\varphi T_z}\int_{-\frac{T_\varphi}{2}}^{\frac{T_\varphi}{2}}\int_{-\frac{T_z}{2}}^{\frac{T_z}{2}} \tilde{J}_z(\varphi,z)\, e^{-j\alpha_m\varphi} e^{-j\beta_n z} d\varphi dz$$

As a result, the given current distribution can be considered as a superposition of current sheets that are sinusoidal both in time and space.
The profile of the current sheet can be obtained by summing four ramps at different axial and azimuth positions. Exploiting the well known property of the Fourier transform:

$$f(x) \Rightarrow F(j\zeta) \text{ and } f(x-x_0) \Rightarrow F_1(j\zeta) = F(j\zeta)\, e^{-j\zeta x_0},$$

it is possible to find the coefficients K'^{φ}_{mn} and K'^{z}_{mn} in (2) as:

$$\begin{aligned}K'^{\varphi}_{mn} =& K^{\varphi}_{mn} e^{-j\alpha_m c_\varphi} e^{-j\beta_n k_z} = \\ &= J\cdot\left[\frac{1}{T_\varphi}\frac{1}{\Delta_\varphi}\frac{2}{(-j\alpha_m)^2}\left(\cos\left(\alpha_m\left(\varphi_0+\frac{\Delta_\varphi}{2}\right)\right)+\right.\right. \\ &\left.\left.-\cos\left(\alpha_m\left(\varphi_0-\frac{\Delta_\varphi}{2}\right)\right)\right)\right]\times \\ &\times\left[\frac{1}{T_z}\frac{2}{j\beta_n}\left(\cos\left(\beta_n\left(z_0+\frac{\Delta_z}{2}\right)\right)+\right.\right. \\ &\left.\left.-\cos\left(\beta_n\left(z_0-\frac{\Delta_z}{2}\right)\right)\right)\right] e^{-j\alpha_m c_\varphi} e^{-j\beta_n k_z}\end{aligned} \tag{3}$$

and:

$$\begin{aligned}K'^{z}_{mn} =& K^{z}_{mn} e^{-j\alpha_m c_\varphi} e^{-j\beta_n k_z} = \\ &= J\cdot\left[-\frac{1}{T_\varphi}\frac{2}{j\alpha_m}\left(\cos\left(\alpha_m\left(\varphi_0+\frac{\Delta_\varphi}{2}\right)\right)+\right.\right. \\ &\left.\left.-\cos\left(\alpha_m\left(\varphi_0-\frac{\Delta_\varphi}{2}\right)\right)\right)\right]\times \\ &\times\left[\frac{1}{T_z}\frac{1}{\Delta_z}\frac{2}{(-j\beta_n)^2}\left(\cos\left(\beta_n\left(z_0+\frac{\Delta_z}{2}\right)\right)+\right.\right. \\ &\left.\left.-\cos\left(\beta_n\left(z_0-\frac{\Delta_z}{2}\right)\right)\right)\right] e^{-j\alpha_m c_\varphi} e^{-j\beta_n k_z}\end{aligned} \tag{4}$$

In order to preserve the consistency of the mathematical model, the divergence of the current sheet must be zero. Substituting (3) and (4) in (2), and then in (5):

$$\nabla\cdot\mathbf{J}(\varphi,z,t) = 0; \tag{5}$$

$$\Downarrow$$

$$\underbrace{\frac{\partial\tilde{J}_r(\varphi,z)}{\partial r}}_{=0} + \underbrace{\frac{\tilde{J}_r(\varphi,z)}{r}}_{=0} + \frac{1}{r}\frac{\partial\tilde{J}_\varphi(\varphi,z)}{\partial\varphi} + \frac{\partial\tilde{J}_z(\varphi,z)}{\partial z} = 0$$

we find:

$$r_0\Delta_\varphi = \Delta_z \tag{6}$$

that is: if the width of the current ribbon along the φ and z directions has the same value, then the condition of null divergence is satisfied. Furthermore, this condition is automatically verified by the adopted current shape in correspondence of the corners (two overlapping ramps as shown in Fig. 2(b)).

III. Formulation in Terms of SOVP

The governing equation in terms of magnetic vector potential constrained by the Coulomb gauge ($\nabla\cdot\mathbf{A} = 0$) for linear isotropic medium is the Poisson's Equation:

$$\nabla^2\mathbf{A} = -\mu\sigma\frac{\partial\mathbf{A}}{\partial t} \tag{7}$$

Since the exciting current is harmonic with respect to the time, the magnetic vector potential will be harmonic too; we can write:

$$\mathbf{A}(r,\varphi,z,t) = \tilde{\mathbf{A}}(r,\varphi,z)\cdot e^{j(\omega-\beta_n v_z)t} \tag{8}$$

and as a consequence:

$$\frac{\partial}{\partial t}\left(\mathbf{A}(r,\varphi,z,t)\right) = j(\omega-\beta_n v_z)\cdot\mathbf{A}(r,\varphi,z,t) \tag{9}$$

it is possible to rewrite the Poisson's equation in the form of the well known Helmholtz's Equation:

$$\nabla^2\tilde{\mathbf{A}} + k^2\tilde{\mathbf{A}} = 0 \tag{10}$$

where $k^2 = -j\mu\sigma(\omega-\beta_n v_z)$ has been assumed.

When dealing with 3D problems and especially in curvilinear coordinates, the separation of variables is not always possible. In these cases the use of the "second-order magnetic potential" $\tilde{\mathbf{W}}$ is the most appropriate way to solve the problem. Since $\nabla\cdot\tilde{\mathbf{A}} = 0$, then: $\tilde{\mathbf{A}} = \nabla\times\tilde{\mathbf{W}}$, where:

$$\tilde{\mathbf{W}} = \tilde{W}_a\mathbf{a}_z + \mathbf{a}_z\times\nabla\tilde{W}_b \tag{11}$$

then, substituting (11) in (10), we have:

$$\nabla \times \left[\left(\nabla^2 \tilde{W}_a + k^2 \tilde{W}_a \right) \mathbf{a}_z + \mathbf{a}_z \times \nabla \left(\nabla^2 \tilde{W}_b + k^2 \tilde{W}_b \right) \right] = 0$$

and finally:

$$\nabla^2 \tilde{W}_a + k^2 \tilde{W}_a = 0 \tag{12}$$
$$\nabla^2 \tilde{W}_b + k^2 \tilde{W}_b = 0 \tag{13}$$

that is: the vector Helmholtz's Equation is replaced by two scalar equations of the same form, in terms of second-order magnetic potentials $\tilde{W}_a$ and $\tilde{W}_b$.

The knowledge of $\tilde{\mathbf{W}}$ in the regions of interest (characterized by different values of electrical conductivity) allows the knowledge of all the electromagnetic quantities. In particular:

$$\tilde{\mathbf{A}} = \nabla \times \tilde{\mathbf{W}} = \begin{cases} \tilde{A}_r = \dfrac{1}{r} \dfrac{\partial \tilde{W}_a}{\partial \varphi} - \dfrac{\partial^2 \tilde{W}_b}{\partial r \partial z}; \\ \tilde{A}_\varphi = -\dfrac{\partial \tilde{W}_a}{\partial r} - \dfrac{1}{r} \dfrac{\partial^2 \tilde{W}_b}{\partial \varphi \partial z}; \\ \tilde{A}_z = \dfrac{\partial^2 \tilde{W}_b}{\partial r^2} + \dfrac{1}{r} \dfrac{\partial \tilde{W}_b}{\partial r} + \dfrac{1}{r^2} \dfrac{\partial^2 \tilde{W}_b}{\partial \varphi^2}; \end{cases} \tag{14}$$

$$\tilde{\mathbf{B}} = \nabla \times \tilde{\mathbf{A}} = \begin{cases} \tilde{B}_r = \dfrac{\partial^2 \tilde{W}_a}{\partial r \partial z} - \dfrac{k^2 \partial \tilde{W}_b}{r \partial \varphi}; \\ \tilde{B}_\varphi = \dfrac{1}{r} \dfrac{\partial^2 \tilde{W}_a}{\partial \varphi \partial z} + k^2 \dfrac{\partial \tilde{W}_b}{\partial r}; \\ \tilde{B}_z = \dfrac{\partial^2 \tilde{W}_a}{\partial z^2} + k^2 \tilde{W}_b; \end{cases} \tag{15}$$

Because of the cylindrical symmetry of the geometry and of the harmonic behaviour of the currents in both axial and azimuth direction, we can assume the following form of the solution of the two scalar equations (12) and (13):

$$\tilde{W}_a(r, \varphi, z) = \hat{W}_a(r) e^{jf(\varphi, z)} \tag{16}$$
$$\tilde{W}_b(r, \varphi, z) = \hat{W}_b(r) e^{jf(\varphi, z)} \tag{17}$$

where: $f(\varphi, z) = \alpha_m (\varphi - c_\varphi) + \beta_n (z - c_z)$.

In cylindrical coordinates system, the Helmholtz's Equations (12) and (13) become:

$$\frac{\partial^2 \tilde{W}_a}{\partial r^2} + \frac{1}{r} \frac{\partial \tilde{W}_a}{\partial r} + \left(\xi_n^2 - \frac{\alpha_m^2}{r^2} \right) \tilde{W}_a = 0 \tag{18}$$

$$\frac{\partial^2 \tilde{W}_b}{\partial r^2} + \frac{1}{r} \frac{\partial \tilde{W}_b}{\partial r} + \left(\xi_n^2 - \frac{\alpha_m^2}{r^2} \right) \tilde{W}_b = 0 \tag{19}$$

where: $\xi_n^2 = k^2 - \beta_n^2$.

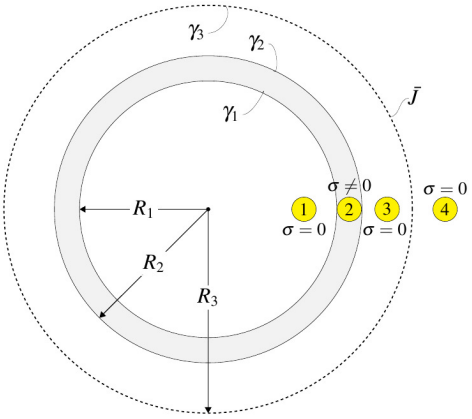

Fig. 3. Schematic view of the domain of interest, divided in four regions.

It is worthwhile to observe that similar equations would have been obtained by assuming moving conductor and coil at rest.

In the domain of interest, divided into four regions has shown in Fig. 3, the solutions of the previous equations are given in terms of Bessel's functions [12].

In the region ② with $\sigma \neq 0$ ($i = 2$):

$$\tilde{W}_a = \sum_{m=-\infty}^{+\infty} \sum_{n=-\infty}^{+\infty} \left[C_{ia} J_{\alpha_m}(\xi_n r) + C'_{ia} Y_{\alpha_m}(\xi_n r) \right] \cdot e^{jf(\varphi, z)} \tag{20}$$
$$\tilde{W}_b = \sum_{m=-\infty}^{+\infty} \sum_{n=-\infty}^{+\infty} \left[C_{ib} J_{\alpha_m}(\xi_n r) + C'_{ib} Y_{\alpha_m}(\xi_n r) \right] \cdot e^{jf(\varphi, z)}$$

while in the regions ①, ③, ④ with $\sigma = 0$ ($i = 1, 3, 4$):

$$\tilde{W}_a = \sum_{m=-\infty}^{+\infty} \sum_{n=-\infty}^{+\infty} \left[C_{ia} I_{\alpha_m}(\beta_n r) + C'_{ia} K_{\alpha_m}(\beta_n r) \right] e^{jf(\varphi, z)} \tag{21}$$
$$\tilde{W}_b = \sum_{m=-\infty}^{+\infty} \sum_{n=-\infty}^{+\infty} \left[C_{ib} I_{\alpha_m}(\beta_n r) + C'_{ib} K_{\alpha_m}(\beta_n r) \right] \cdot e^{jf(\varphi, z)}$$

where: J_{α_m}, and Y_{α_m}, are the Bessel's functions of order α_m of the first and second kind respectively; I_{α_m}, and K_{α_m} are the modified Bessel's function of order α_m of the first and second kind respectively; C_{ia}, C'_{ia}, C_{ib}, and C'_{ib}, are integration constants which can be calculated from the normal conditions and the boundary conditions on the interfaces γ_1, γ_2, and γ_3 (Fig. 3). Because of the asymptotic behavior of the modified Bessel function we have: $C'_{1a} = C_{4a} = 0$. In order to determine the integration constants in (20) and (21), we have to impose the continuity of the normal component of the magnetic flux density $\tilde{B}_\perp$ across the interfaces $1-2$, $2-3$, and $3-4$. The tangential component of the magnetic field $\tilde{H}_\parallel$ must be continuous across the interfaces $1-2$, and $2-3$; furthermore, $\tilde{H}_\parallel$ is necessarily discontinuous across the interface $3-4$ containing the excitation current sheet:

$$\begin{cases} \tilde{B}_{r_1}(R_1) = \tilde{B}_{r_2}(R_1); & \text{(22a)} \\ \tilde{B}_{r_2}(R_2) = \tilde{B}_{r_3}(R_2); & \text{(22b)} \\ \tilde{B}_{r_3}(R_3) = \tilde{B}_{r_4}(R_3); & \text{(22c)} \\ \frac{1}{\mu_0}\tilde{B}_{\varphi_1}(R_1) = \frac{1}{\mu_0\mu_r}\tilde{B}_{\varphi_2}(R_1); & \text{(22d)} \\ \frac{1}{\mu_0}\tilde{B}_{z_1}(R_1) = \frac{1}{\mu_0\mu_r}\tilde{B}_{z_2}(R_1); & \text{(22e)} \\ \frac{1}{\mu_0}\tilde{B}_{\varphi_2}(R_2) = \frac{1}{\mu_0\mu_r}\tilde{B}_{\varphi_3}(R_2); & \text{(22f)} \\ \frac{1}{\mu_0}\tilde{B}_{z_2}(R_2) = \frac{1}{\mu_0\mu_r}\tilde{B}_{z_3}(R_2); & \text{(22g)} \\ \frac{1}{\mu_0}\tilde{B}_{\varphi_3}(R_3) = \frac{1}{\mu_0\mu_r}\tilde{B}_{\varphi_4}(R_3) + \tilde{J}_z(R_3); & \text{(22h)} \\ \frac{1}{\mu_0}\tilde{B}_{z_3}(R_3) = \frac{1}{\mu_0\mu_r}\tilde{B}_{z_4}(R_3) + \tilde{J}_\varphi(R_i); & \text{(22i)} \end{cases}$$

where: $\tilde{\mathbf{H}} = \frac{1}{\mu_0\mu_r}\tilde{\mathbf{B}}$.

Let us observe that the potential $\tilde{W}_b$ contributes to the expression of the solution in the conductive region only. Once normal conditions have been considered, eight integration constants have to be determined by imposing the above equations whose total number is nine. However, under the condition $r_0\Delta_\varphi = \Delta_z$ we will demonstrate that the last two boundary conditions involving the discontinuity of the magnetic field strength (eqs. (22h) and (22i)) are not linearly independent. This implies that one of them can be discarded. Expressing the components of $\tilde{\mathbf{B}}$ in terms of SOVPs it yields:

$$\tilde{B}_{\varphi_3}(R_3) = \frac{1\partial^2\tilde{W}_{a_3}}{r\,\partial\varphi\partial z} = -\frac{1}{R_3}\alpha_m\beta_n\tilde{W}_{a_3}; \quad \text{(23a)}$$

$$\tilde{B}_{\varphi_4}(R_3) = \frac{1\partial^2\tilde{W}_{a_4}}{r\,\partial\varphi\partial z} = -\frac{1}{R_3}\alpha_m\beta_n\tilde{W}_{a_4}; \quad \text{(23b)}$$

$$\tilde{B}_{z_3}(R_3) = \frac{\partial^2\tilde{W}_{a_3}}{\partial z^2} = -\beta_n^2\tilde{W}_{a_3} \quad \text{(23c)}$$

$$\tilde{B}_{z_4}(R_3) = \frac{\partial^2\tilde{W}_{a_4}}{\partial z^2} = -\beta_n^2\tilde{W}_{a_4} \quad \text{(23d)}$$

(24)

and substituting in (22h) and (22i), we have:

$$\begin{cases} \frac{1}{\mu_0}\frac{1}{R_3}\alpha_m\beta_n\left(\tilde{W}_{a_4} - \tilde{W}_{a_3}\right) = \tilde{J}_z & \text{(25a)} \\ \frac{1}{\mu_0}\beta_n^2\left(\tilde{W}_{a_4} - \tilde{W}_{a_3}\right) = \tilde{J}_\varphi & \text{(25b)} \end{cases}$$

Then, dividing (25a) by (25b) and recalling (2), we can write:

$$\frac{\frac{1}{\mu_0}\frac{1}{R_3}\alpha_m\beta_n\cdot\left(\tilde{W}_{a_4} - \tilde{W}_{a_3}\right)}{\frac{1}{\mu_0}\beta_n^2\cdot\left(\tilde{W}_{a_4} - \tilde{W}_{a_3}\right)} = \frac{\tilde{J}_z}{\tilde{J}_\varphi} = \frac{K'^{z}_{mn}}{K'^{\varphi}_{mn}} \quad \text{(26)}$$

Finally, taking into account (3), (4) and (6), eq. (26) gives:

$$\frac{\alpha_m}{R_3\cdot\beta_n} = \frac{\alpha_m\Delta\varphi}{\beta_n\cdot\Delta z} \quad \Longrightarrow \quad 1 = 1 \quad q.e.d. \quad \text{(27)}$$

The remaining eight equations can be solved to obtain the eight integration constants C_{1a}, C_{2a}, C'_{2a}, C_{2b}, C'_{2b}, C_{3a}, C'_{3a}, and C'_{4a}.

All the electromagnetic quantities of interest can be evaluated; in particular, the induced eddy currents are found as:

$$\tilde{\mathbf{J}} = \sigma\tilde{\mathbf{E}} = -j\sigma(\omega - \beta_n v_z)\cdot\tilde{\mathbf{A}}; \quad \text{(28)}$$

and the total thrust force is obtained by:

$$F = \frac{1}{2}\int_V \Re\left(\tilde{\mathbf{J}}\times\tilde{\mathbf{B}}^*\right)dv; \quad \text{(29)}$$

where V is the conductive cylinder.

IV. Application example

We considered an infinitely long cylinder (see Fig. 4) with internal radius $R_1 = 5.1\ cm$ and external one $R_2 = 6.1\ cm$. Eight equally spaced coils are distributed in the azimuth direction on a cylinder with a radius $R_3 = 6.45\ cm$; this configuration is repeated 12 times along the axial direction. The width of the coil is $\triangle z = R_3\triangle\varphi = 6.0\ mm$ and the average length of both the sides is $\Delta\ell = 24\ mm$. The distance along the axial direction of the centers of two adjacent coils is $L_z = 4.2\ cm$.

The coils sharing the same axial position characterized by z_n are fed with the current $i(t) = I_M\sin(\omega_0 t - k(z_n - z_0))\ [A]$, with $I_M = 50\ kA$, $\omega_0 = 314.16\ rad/s$, $k = 2\pi/(6\cdot 0.042) = 24.933\ m^{-1}$, while z_0 is the position of the first group of coils. A travelling wave of magnetic flux density with two pole pairs moves in the axial direction at the speed $v_s = \omega_0/k = 12.6\ m/s$. If v_z is the speed of the mover, the slip is defined as: $s = (v_s - v_z)/v_s$. We evaluated the current density distribution on the cylinder and the thrust force on it in correspondence to $s = 1$ and $s = 0.5$.

Results

Fig. 5 shows the current distribution at the average radius of the cylinder. The vertical axis indicates the distance taken on the azimuth direction from a line parallel to the axis and located in the middle of two adjacent arrays of coils. The distribution on one quarter of the cylinder is shown.
Fig. 6 shows the current density components along a line parallel to the z-axis in correspondence of the centers of the portion of the coils whose current is directed along the z-axis. The presence of two pole pairs is easily identified. The thrust force on the mover evaluated by eq. (29) is $F = 3.4\ kN$. Fig. 7 shows the current density in the same region as in Fig. 5 but in correspondence of $s = 0.5$, while Fig. 8 shows the same quantity as Fig. 6.

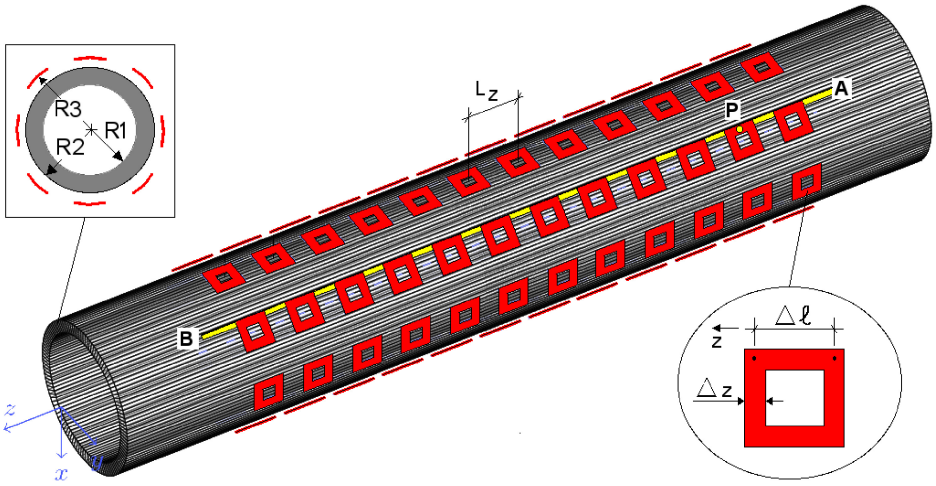

Fig. 4. Application example.

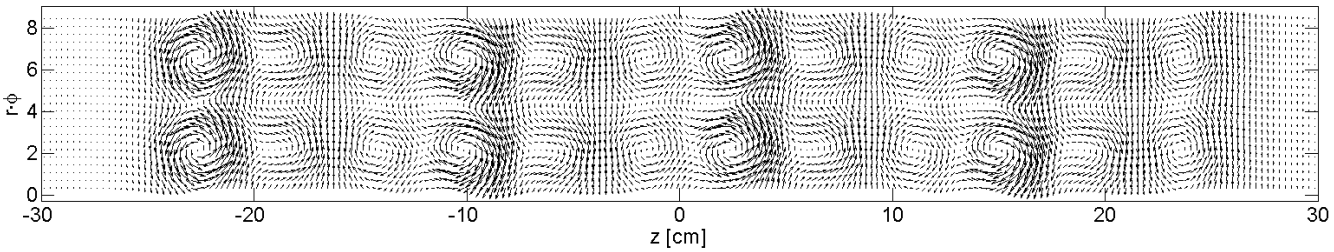

Fig. 5. Current density distribution on one quarter of the cylindrical surface: $s = 1$.

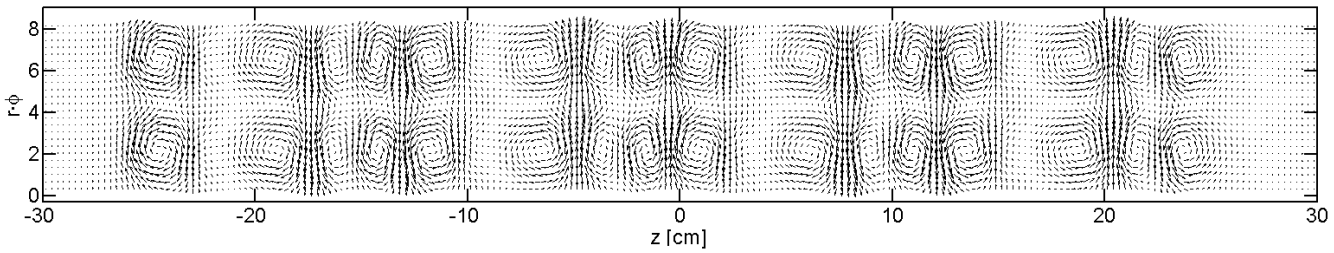

Fig. 7. Current density distribution on one quarter of the cylindrical surface: $s = 0.5$.

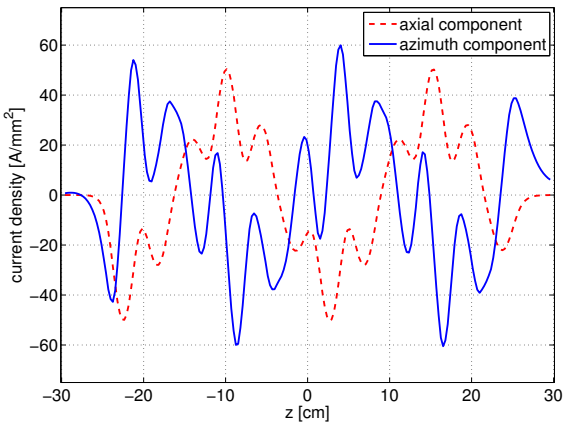

Fig. 6. Distribution of the current density on a line $A - B$ (see fig. 4) parallel to the axis of the cylinder under the stright side of the coil ($s = 1$).

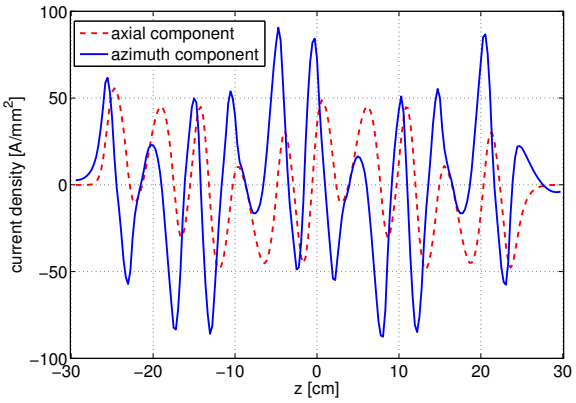

Fig. 8. Distribution of the current density on a line $A-B$ (see fig. 4) parallel to the axis of the cylinder under the stright side of the coil ($s = 0.5$).

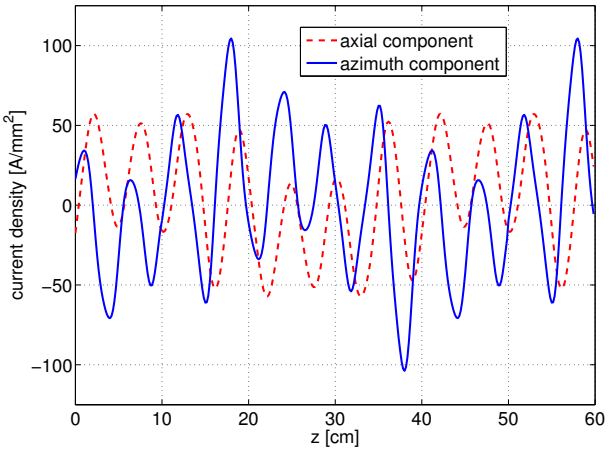

Fig. 9. Time waveform of the current densities on a point P (see fig. 4) on the conductive cylinder ($s = 0.5$).

Fig. 9 reports the waveforms with respect to the time of the axial and azimuth components of the current density on a point on the cylinder. At $t = 0$ this point (labeled with P in fig. 4) was in correspondence of the middle of the stright side of one of the coils in the second ring. As expected because of the slip $s = 0.5$ the frequency of the fundamental of these waveforms is halved with respect to the frequency $f = 50\ Hz$ of the exciting currents. The thrust force on the cylinder is $F = 12.0\ kN$. The results have been compared with those obtained by an integral formulation described in [13] - [18], showing an excellent agreement. It is worthwhile to note that the equivalent circuit adopted in the above formulation allows for a quick and accurate evaluation of the sensitivity with respect to the design parameters [19]. This may be a valuable help in the design of the device when optimization by gradient based methods is adopted.

TABLE I
COIL DIMENSIONS

Coil type	L_z $[cm]$	$\Delta\ell$ $[mm]$	Δz $[mm]$	F_z $(s = 0.5)$ $[kN]$	F_z $(s = 1)$ $[kN]$
♯1	4.2	24	6	12.2	3.45
♯2	4.2	22	8	10.9	3.08
♯3	4.2	26	4	12.6	3.25
♯4	4.2	18	4	9.65	2.77
♯5	4.2	20	6	10.6	2.85

simulations maintaining the same armature characteristics, the same distance L_z between the coils, while varying $\Delta\ell$ and Δ_z according to table I.

Figs. 10 and 11 show the current distribution on the cylindrical surface in correspondence of excitation system based on coil ♯1 and ♯4 respectively. As reported in table I, the thrust force on the armature is the highest with coil ♯1 and the lowest with coil ♯4.

Figs. 12 and 13 show the comparison of the azimuth and axial component of the current density along a line parallel to the line $A - B$ (see fig. 4) at a radius $r = 5.925\ cm$ and an angle of 9^o with respect to the middle line between two adjacent coils in the azimuth direction. The results have been obtained at slip $s = 0.5$.

Figs. 14 and 15 show the same quantities obtained at a slip $s = 1$. It is worth to observe that in both cases ($s = 0.5$ and $s = 1$), the highest force corresponds to the most intense current density (the one marked with circles). Similarly the lowest force correspond to the weakest current density marked by squares.

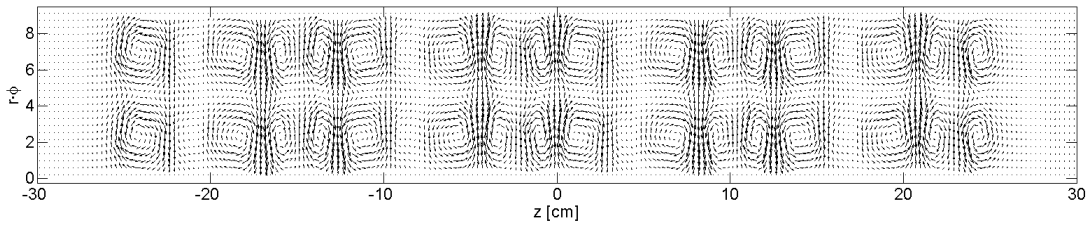

Fig. 10. Current density distribution on one quarter of the cylindrical surface: $s = 0.5$ with coil ♯1.

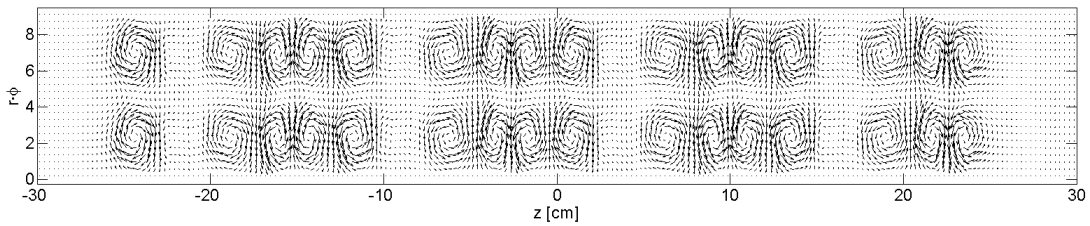

Fig. 11. Current density distribution on one quarter of the cylindrical surface: $s = 0.5$ with coil ♯4.

We also consider the effect of changes in the excitation coil geometry. With reference to the inset of Fig. 4, which describes the coil geometry, we performed a number of

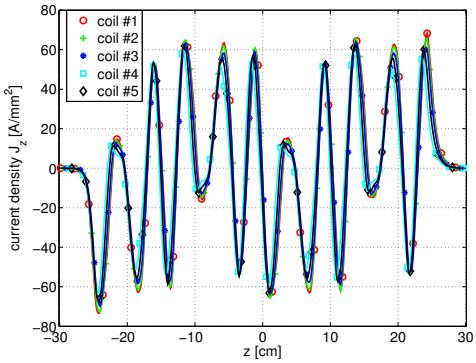

Fig. 12. Comparison of the armature current density @ $s = 0.5$.

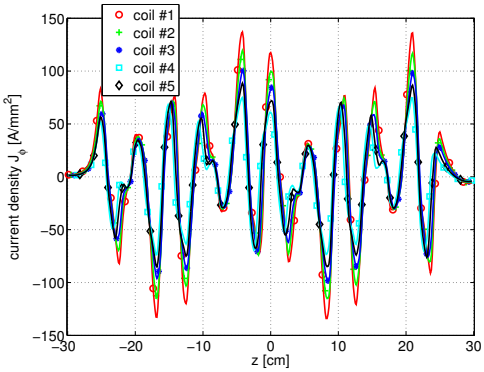

Fig. 13. Comparison of the armature current density @ $s = 0.5$.

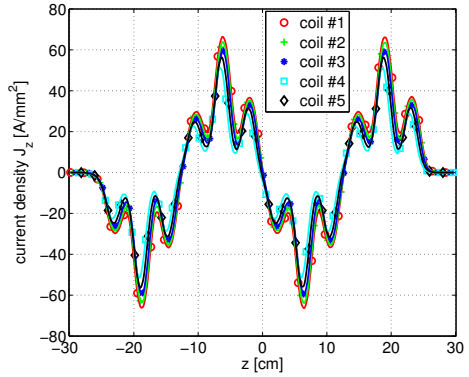

Fig. 14. Comparison of the armature current density @ $s = 1$.

V. Conclusion

An analytical model for the evaluation of the eddy current induced in a conductive cylinder by a set of saddle shaped coils moving in the axial direction has been considered. The problem has been approached by a double Fourier transform and the SOVP; the solution has been expressed in terms of a double series of Bessels functions. The proposed model has been used to analyzed a recently proposed induction launcher named multipole field electromagnetic launcher in its travelling wave configuration.

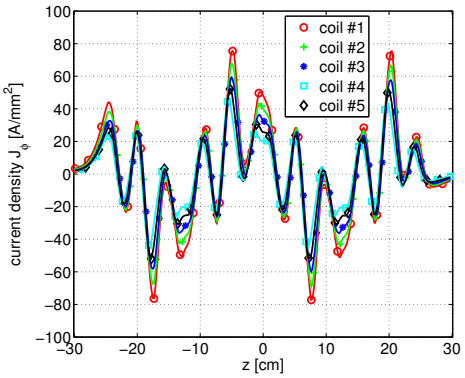

Fig. 15. Comparison of the armature current density @ $s = 1$.

References

[1] Yingwei Zhu, Yu Wang, Zhongming Yan, Liang Dong, Xiaofang Xie, and Haitao Li, "Multipole Field Electromagnetic Launcher", IEEE Trans. on Magn., vol. 46, pp. 26222627, Jun. 2010.

[2] Zhu Yingwei; Wang Yu; Chen Weirong; Yan Zhongming; Li Haitao, "Analysis and Evaluation of Three-Stage Twisty Octapole Field Electromagnetic Launcher", IEEE Trans. on Plasma Sci., Vol. 40, n. 5, pp. 1399-1406, 2012.

[3] M. Cowan, E. Cnare, B. Duggin, R. Kaye, T. Tucker, "The reconnection gun" IEEE Trans. Magn., vol. 22, n. 6, pp. 1429 - 1434, Nov. 1986.

[4] J. H. He, E. Levi, Z. Zabar, L. Birembaum, and Y. Naot, "Analysis of induction-type coilgun performance based on cylindrical current sheet model", IEEE Trans. Magn., vol. 27, pp. 579584, Jan. 1991.

[5] Barmada, S., Musolino, A., Raugi, M., Rizzo, R., "Numerical simulation of a complete generator-rail launch system", IEEE Trans. on Magn., vol. 41, n. 1, pp. 369-374, 2005.

[6] J. A. Tegopulos, and E. E: Kriezis, "Eddy Currents in Linear Conducting Media", Amsterdam: Elsevier, 1985.

[7] W. R. Smythe, "Static and Dynamic Electricity". NY, McGraw-Hill, 1968.

[8] P. Hammond, "Use of potentials in calculation of electromagnetic fields", Inst. Elect. Eng. Proc. Pt. A, vol. 129, no. 2, pp. 106112, Mar. 1982.

[9] T. P. Theodoulidis, N. V Kantartzis, T. D Tsiboukis, and E. E Kriezis, "Analytical and Numerical Solution of the Eddy-Current Problem in Spherical Coordinates Based on the Second-Order Vector Potential Formulation", IEEE Trans. Magn., vol. 33, n. 4, pp. 24612472, July 1997.

[10] Barmada, S., Musolino, A., Raugi, M., Rizzo, R., "Analysis of the performance of a combined coil-rail launcher", IEEE Trans. on Magn., vol. 39, n. 1, pp. 103-107, 2003.

[11] Musolino, A., Rizzo, R., Tucci, M., Matrosov, V.M., "A new passive maglev system based on eddy current stabilization", IEEE Trans. on Magn., vol. 45, n. 3, pp. 984-987, 2009.

[12] M. Abramovitz, and I. A. Stegun, Handbook of Mathematical Functions, New York: Dover, 1972.

[13] Musolino, A., Rizzo, R., "Numerical analysis of brush commutation in helical coil electromagnetic launchers", IET Science, Measurement and Technology, vol. 5, n. 4, pp. 147-154, 2011.

[14] Musolino, A., Rizzo, R., "Numerical modeling of helical launchers", IEEE Trans. on Plasma Sci., vol. 39, pp. 935-940, 2011.

[15] Musolino, A., "Numerical analysis of a rail launcher with a multilayered armature", IEEE Trans. on Plasma Sci., vol. 39, pp. 788-793, 2011.

[16] Musolino A., Rizzo. R., Toni M., Tripodi E., "Modelling of electromechanical devices by GPU accelerated integral formulation", J. of Num. Modelling: Electron. Networks, Devices and Fields, 2012, Published online in Wiley Online Library (wileyonlinelibrary.com). DOI:10.1002/jnm.1860, pp 1-21.

[17] A. Musolino, R. Rizzo, E. Tripodi "Analysis and Design Criteria of a Tubular Linear Induction Motor for a Possible Use in the Electro-Magnetic Aircraft Launch System", IEEE 16th EML Symposium Conf. Proceedings, May 15-19 Beijing, 2012.

[18] A. Musolino, R. Rizzo. M. Toni, E. Tripodi, "Acceleration of Electromagnetic Launchers Modeling by Using Graphic Processing Unit", IEEE 16th EML Symposium Conf. Proceedings, May 15-19 Beijing, 2012.

[19] Barmada, S., Musolino, A., Rizzo, R., Tucci, M., "Multi-resolution based sensitivity analysis of complex non-linear circuits", IET Circuits, Devices and Systems, vol. 6, n. 3, pp. 176-186, 2012.